LASER
& PHOTONICS
REVIEWS

Supporting Information

for *Laser Photonics Rev.*, DOI 10.1002/lpor.202300850

Manipulating the Exciton Dynamics in a MoS_2/WS_2 Heterobilayer with a Si/Au Nanocavity

*Shimei Liu, Shulei Li, Yuheng Mao, Zhenxu Lin, Mingcheng Panmai, Guang-Can Li, Lidan Zhou and Sheng Lan**

Supporting Information

Manipulating the exciton dynamics in a MoS_2/WS_2 heterobilayer with a Si/Au nanocavity

*Shimei Liu, Shulei Li, Yuheng Mao, Zhenxu Lin, Mingcheng Panmai, Guang-Can Li, Lidan Zhou, and Sheng Lan**

S. Liu, Y. Mao, Z. Lin, G. Li, S. Lan
Guangdong Provincial Key Laboratory of Nanophotonic Functional Materials and Devices
School of Information and Optoelectronic Science and Engineering
South China Normal University
Guangzhou 510006, P. R. China
E-mail: slan@scnu.edu.cn
S. Li
School of Optoelectronic Engineering
Guangdong Polytechnic Normal University
Guangzhou 510665, P. R. China
M. Panmai
School of Electrical and Electronic Engineering
Nanyang Technological University
Singapore 639798, Singapore
L. Zhou
State Key Laboratory of Optoelectronic Materials and Technologies
School of Electronics and Information Technology
Sun Yat-sen University
Guangzhou 51006, P. R. China

Supplementary Note 1

Since a type II heterostructure is generally created by a heterobilayer composed of TMDCs, efficient charge transfer in the heterobilayer will lead to the separation of electrons and holes in the two constituent TMDCs upon optical excitation. As a result, the PL from the heterobilayer is dramatically quenched. In Figure S1, we compared the PL spectra of a MoS_2/WS_2 HB attached on a thin Au film without (blue curve) and with (red curve) a Si nanoparticle (No. 1). The PL spectra of a MoS_2 (green curve) and a WS_2 (black curve) monolayer are also provided for reference. It can be seen that the PL intensity of the WS_2 monolayer is much stronger than that of the MoS_2 monolayer. It means that the PL of a MoS_2/WS_2 HB is dominated by the PL of the WS_2 monolayer. In addition, it is noticed that the PL from the MoS_2/WS_2 HB is greatly reduced as compared with that of the WS_2 monolayer. Since the plasmon resonance of the Si/Au nanocavity (~590 nm) is far away from the exciton resonance of the WS_2 monolayer (~615 nm), the PL of the MoS_2/WS_2 HB is reduced in the presence of the Si nanoparticle due to the strain effect. For another Si/Au nanocavity (No. 4) with its plasmon resonance (~626 nm) close to the exciton/trion resonance, one can see the PL enhancement of the MoS_2/WS_2 HB in the presence of the Si nanoparticle.

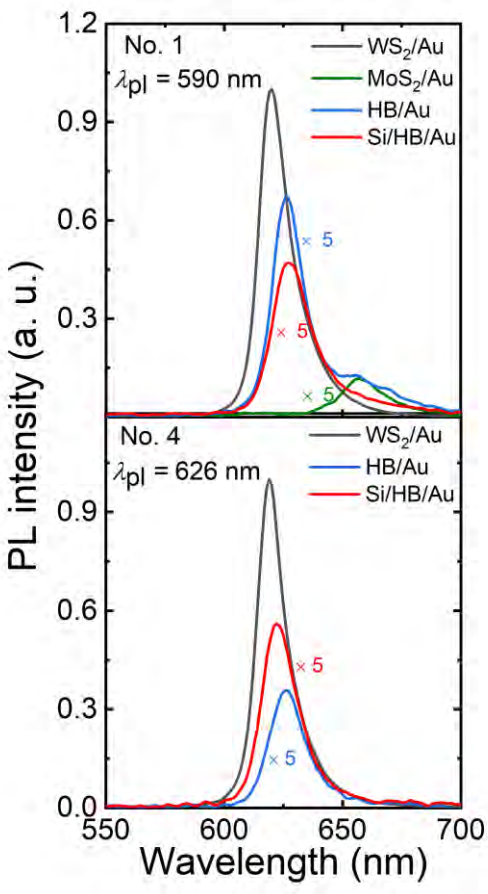

Figure S1. PL spectra measured for two different Si/HB/Au nanocavities at a laser power of P = 32 μW (red solid curves). In each case, the PL spectra of a MoS_2 monolayer (green curve), a WS_2 monolayer (black curve), and a HB/Au (blue curve) measured under the same conditions are also provided for comparison.

Supplementary Note 2

The relationship between the adhesion force F and the Hamaker constant A is described as follows:[1,2]

$$F = \frac{AR}{6D^2}, \tag{1}$$

where R and D represent curvature radius and interaction distance between the two surfaces, respectively. Theoretically, the Hamaker constant A of a dielectric-dielectric interaction can be expressed as:[2]

$$A = \frac{3}{4}kT\left(\frac{\varepsilon_1-\varepsilon_3}{\varepsilon_1+\varepsilon_3}\right)\left(\frac{\varepsilon_2-\varepsilon_3}{\varepsilon_2+\varepsilon_3}\right)+\frac{3h\nu_e}{8\sqrt{2}}\frac{(n_1^2-n_3^2)(n_2^2-n_3^2)}{\left(\sqrt{n_1^2+n_3^2}\right)\left(\sqrt{n_2^2+n_3^2}\right)\left(\sqrt{n_1^2+n_3^2}+\sqrt{n_2^2+n_3^2}\right)}, \tag{2}$$

where ε_1 (n_1) and ε_2 (n_2) represent the dielectric constants (refractive indices) of the two surfaces, and the ε_3 (n_3) represents the dielectric constant (refractive index) of the gap material. Thus, the adhesion force of a dielectric-dielectric interaction is related to the gap material. In comparison, the Hamaker constant A of a metal-dielectric interaction can be described as:[2]

$$A = \frac{3}{4}kT\left(\frac{\varepsilon_1-1}{\varepsilon_1+1}\right)+\frac{3h\nu_e}{8\sqrt{2}}\frac{(n_1^2-1)}{\left(\sqrt{n_1^2+1}+1\right)\left(\sqrt{n_1^2+1}\right)}, \tag{3}$$

where ε_1 and n_1 represent dielectric constant and refractive index of Si. Thus, the adhesion force of a metal-dielectric interaction is not influenced by the gap material. In Figure S2, we present the dependence of the adhesion force between a Si nanoparticle and an Au film on the interaction distance D and curvature radius R (bule curves). For safety, we also evaluated the adhesion force between a Si nanoparticle and a MoS_2 film (red curves). It appeared to be larger than that between a Si nanoparticle and an Au film. It can be seen that the adhesion force increases rapid with decreasing distance. In addition, it is noticed that the adhesion force is not sensitive to the size of the Si nanoparticle. It should be emphasized that the adhesion force is on the order of nN, which is large enough to induce the deformation of a MoS_2/WS_2 HB via the strain effect.

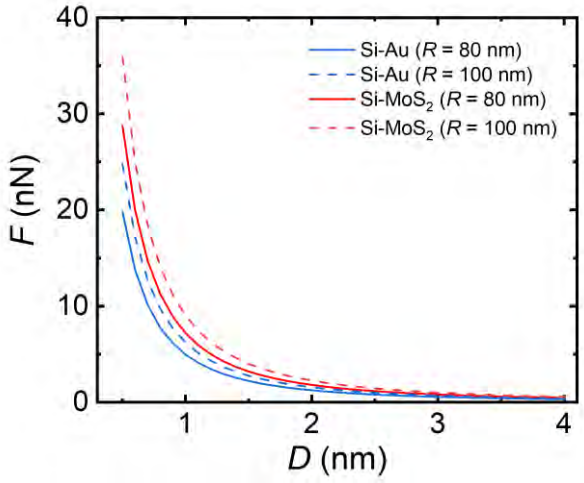

Figure S2. Dependence of the adhesion force (F) between a Si nanoparticle and an Au film (blue curves) on the interaction distance (D) and curvature radius (R). Also shown are the dependences of the adhesion force (F) between a Si nanoparticle and a MoS_2 film (red curves).

Supplementary Note 3

Since the excitons in a WS_2 monolayer oriented mainly in the xy plane, we first examined the distribution of the in-plane electric field intensity ($|E_{xy}/E_0|$) calculated for a Si/HB/Au nanocavity with d = 172 nm, as shown in Figure S3a. In this case, the nanocavity was excited by using a plane wave polarized along the x direction. It should be emphasized that the size of the hot spots (~0.0078 μm^2) is much smaller than that of the laser spot (~1.13 μm^2). Therefore, the enhancement in the PL intensity of the exciton at the presence of a Si nanoparticle may not be significant as expected. In Figure S3b, we show the electric field distribution in the xz plane calculated for the Si/HB/Au nanocavity. One can see the enhanced electric field in the gap between the Si nanoparticle and the Au film. In addition, we examined the wavelength-dependent enhancement factors of the in-plane electric field (i.e., $\int |E_{xy}(\lambda)|^2 dV/V$) averaged over the volume of the MoS_2/WS_2. It determines the emission rate of excitons owing to the Purcell effect. The enhancement factors calculated for Si/Au and Si/HB/Au nanocavities composed of Si nanoparticles with different diameters are shown in Figure S3c,d. It was found that the largest enhancement factor at the exciton resonance (~615 nm) of WS_2 monolayer is achieved in the Si/HB/Au nanocavity with d ~ 176 nm. Therefore, it is expected that the largest PL enhancement is achieved in the Si/HB/Au nanocavity. We also simulated the two-dimensional radiation patterns of HB/Au and Si/HB/Au nanocavity, as shown in Figure 3e,f. It can be seen that the radiation intensity is greatly enhanced in the presence of the Si nanoparticle due to the large Purcell factor.

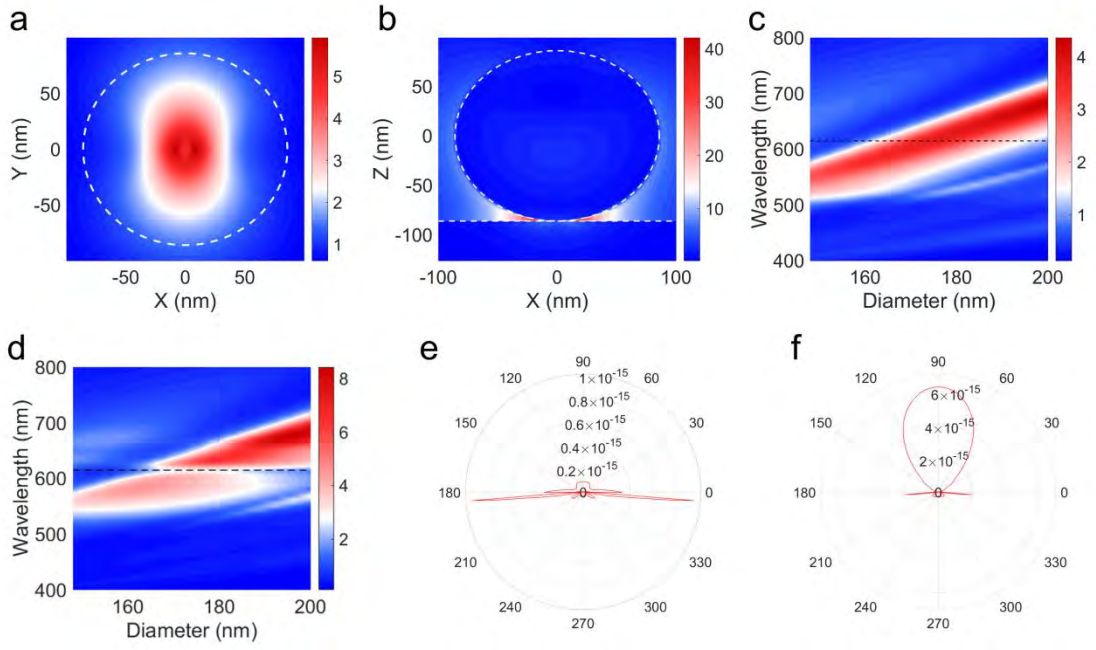

Figure S3. (a) In-plane electric field distribution ($|E_{xy}/E_0|$) and (b) electric field distribution in the xz plane calculated for a Si/HB/Au nanocavity with d = 172 nm at the exciton resonance of WS_2 monolayer (615 nm). (c)(d) In-plane electric field intensities ($\int |E_{xy}(\lambda)|^2 dV/V$) calculated for Si/Au nanocavities and Si/HB/Au nanocavities composed of Si nanoparticles with different diameters. The exciton resonance (615 nm) in WS_2

monolayer is marked by the horizontal line. (e)(f) Radiation patterns in the yz plane calculated for a HB/Au and a Si/HB/Au nanocavity with d = 178 nm.

Supplementary Note 4

In Figure S4a, we show the PL intensity mapping of triangular WS_2 and MoS_2 monolayers obtained by using a single-photon laser scanning confocal microscope. The size of WS_2 monolayers is larger than that of MoS_2 monolayers. It appeared that the PL intensity from the MoS_2 monolayer was even weaker than that from the Au film (the Au/SiO_2 substrate). This abnormal phenomenon cannot be ascribed to the bandpass optical filter (550-720 nm) was used in the measurement. It is suspected that the emission from the MoS_2 monolayer and Au film was reabsorbed by the MoS_2 monolayer. Since PL quenching occurs for a MoS_2/WS_2 HB, one can easily identify MoS_2 monolayers, which appear as dark triangles in the image. Due to the nonuniformity of the HB/Au, there exists a fluctuation in the PL intensities measured at different positions. In Figure S4b, we show the bright-field image of a Si/HB/Au nanocavity (No. 4). The Si nanoparticle used to construct the nanocavity is enclosed by a white circle. We measured the PL spectra of the HB/Au at different positions around the Si nanoparticle, as marked by red circles. The PL spectra measured at these positions and the PL spectrum measured for nanocavity are presented in Figure S4c. Although there exists a fluctuation in the PL intensities measured at different positions, the PL intensity of the Si/HB/Au nanocavity is stronger than those of the HB/Au.

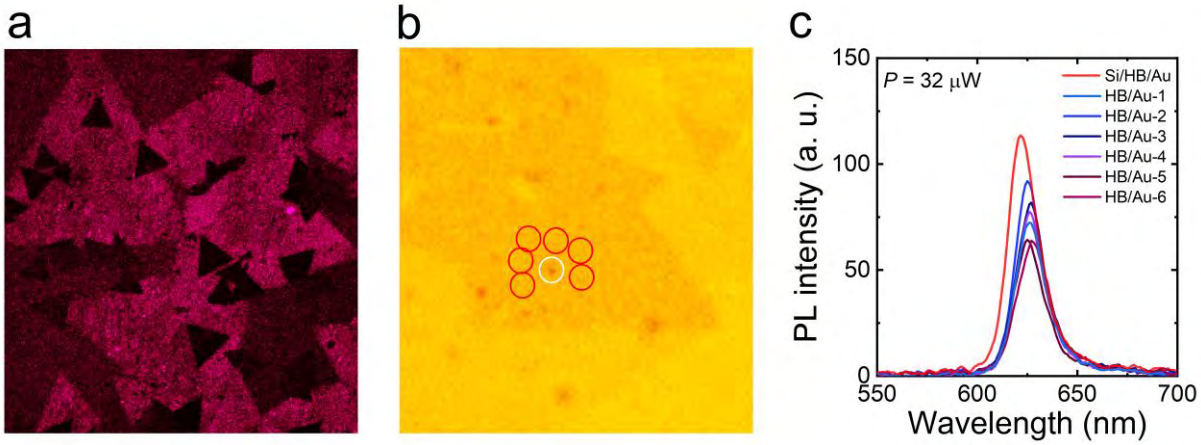

Figure S4. (a) PL intensity mapping of HB/Au. (b) Bright-field image of a Si/HB/Au nanocavity. The Si nanoparticle is enclosed by the white circle. The red circles indicate the positions at which the PL spectra of the HB/Au are examined. (c) PL spectra measured for the HB/Au at different positions and for the Si/HB/Au nanocavity at a laser power of P = 32 μW.

Supplementary Note 5

In Figure S5a, we show a typical SEM image for a WS_2 monolayer, a MoS_2 monolayer, and a MoS_2/WS_2 HB on an Au/SiO_2 substrate. And we didn't observe any strains and grain boundaries, indicating the high-quality of the studied MoS_2/WS_2 HBs. The Raman spectra measured for the MoS_2/WS_2 HB without and with a Si nanoparticle are presented in Figure S5b. The four peaks observed at 350, 380, 403, and 416 cm^{-1} are attributed to the E' and A_1' modes of MoS_2 and WS_2.[3] It is noticed that the intensities of the A_1' mode and 2LA(M) & E' modes of WS_2 are enhanced in the presence of the Si nanoparticle. We also performed AFM measurement for the MoS_2/WS_2 HB, as shown in Figure S5c. Based on the height profile shown in Figure S5d, the height difference between the surface of the MoS_2 monolayer and that of the WS_2 monolayer was found to be ~1.0 nm, quite similar to that reported in the literature.[4] In Figure S5c,d, one can identify the residual polymer left on the surfaces of the MoS_2 and WS_2 monolayers, which may affect the interlayer coupling and the formation of interlayer excitons.[3]

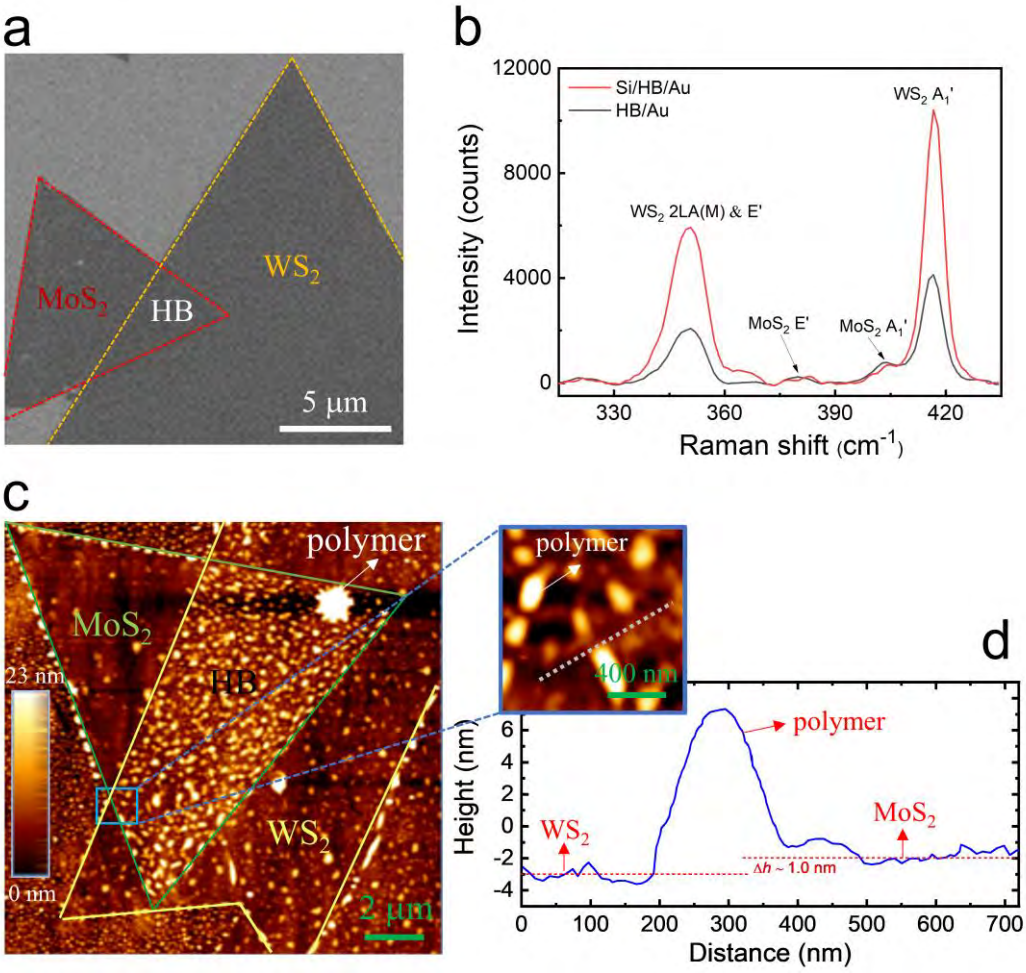

Figure S5. (a) SEM image for a WS_2 monolayer, a MoS_2 monolayer, and a MoS_2/WS_2 HB on an Au/SiO_2 substrate. (b) Raman spectra measured for HB/Au and Si/HB/Au. (c) AFM image for a WS_2 monolayer, a MoS_2 monolayer, and a MoS_2/WS_2 HB on an Au/SiO_2 substrate. (d) Height profile extracted from the dashed line in the magnified AFM image.

Supplementary Note 6

In Figure S6a,b, we show the forward and backward scattering spectra measured for Si/HB/Au nanocavities composed of Si nanoparticles with different diameters (black solid curves). In all cases, the calculated scattering spectra (red dashed curves) are also provided for comparison. In the numerical simulations, the diameters of the Si nanoparticles were based on the SEM observation. Since the Si nanoparticles fabricated by using femtosecond laser ablation may not be spherical, there is a small difference in the peak wavelength of the MMD between the measured and simulated results in some cases. In addition, it was found that the linewidth of the MMD in the measured scattering spectra is narrower than that in the simulated scattering spectra. The reason for this discrepancy is the normally incident wave used in the numerical simulations and the inclined illumination light used in the experimental measurements.[5-7]

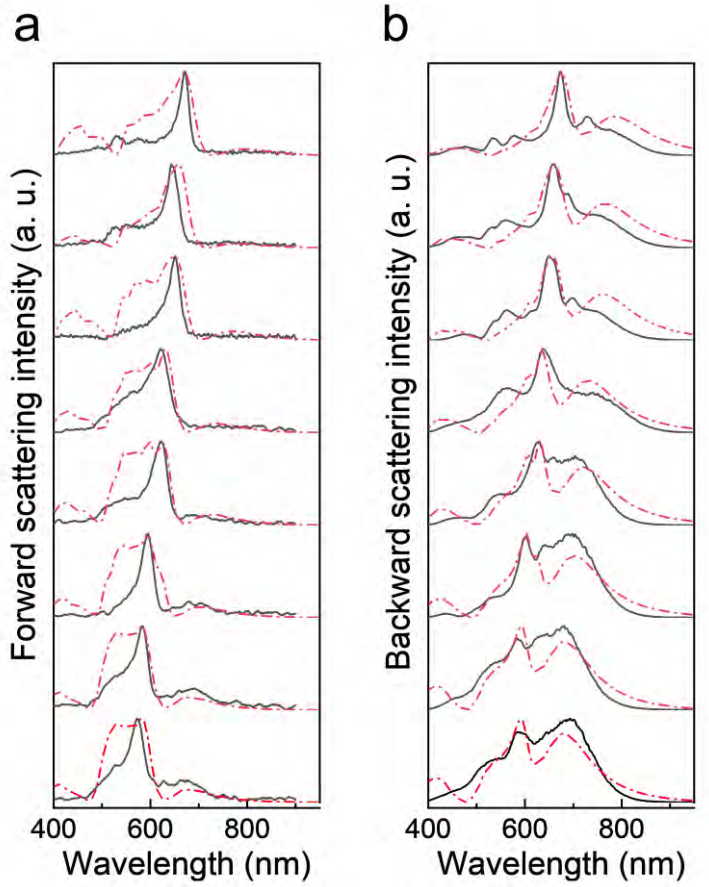

Figure S6. (a)(b) Forward and backward scattering spectra (black solid curves) measured for Si/HB/Au nanocavities. In all cases, the calculated scattering spectra (red dashed curves) are also provided for comparison.

Supplementary Note 7

We measured the PL spectra of Si/HB/Au nanocavities composed of Si nanoparticles with different diameters at different laser powers, as shown in Figure S7. In each case, the PL spectrum of the HB/Au obtained under the same excitation condition is also provided for comparison. For nanocavities composed of Si nanoparticles with small diameters (a, b) and lager diameters (f-g), the PL intensities at all laser powers are weaker than those of the HB/Au. For nanocavities with appropriate diameters (c, d), the PL intensities at all laser powers are stronger than those of the HB/Au. For the nanocavity shown in (e) (No. 5), the PL intensities at low laser powers are weaker than those of the HB/Au. However, the PL intensities at high laser powers become stronger than those of the HB/Au.

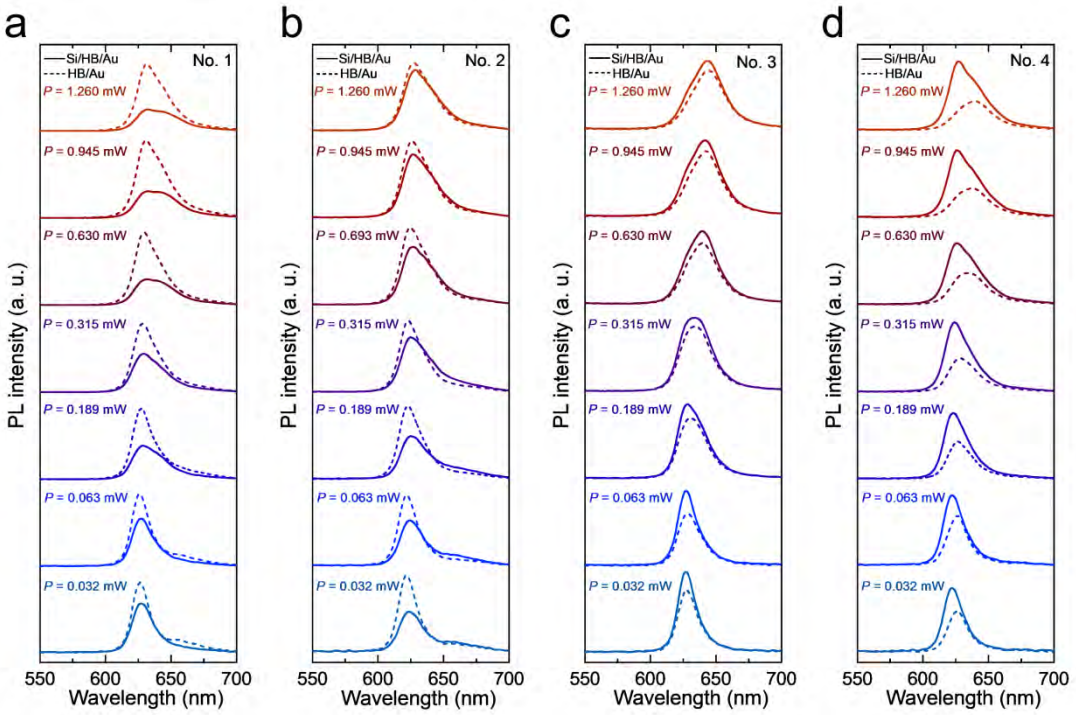

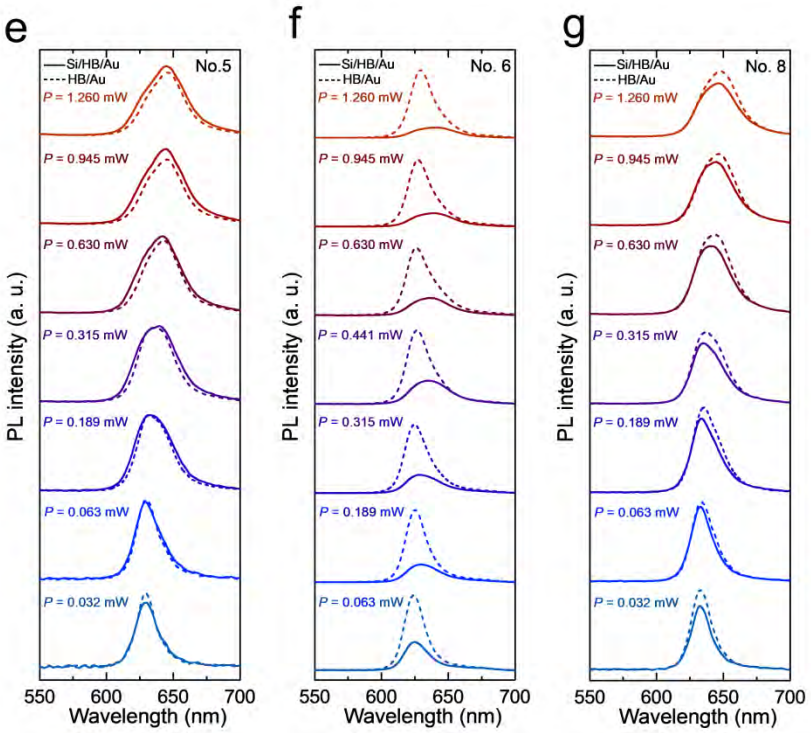

Figure S7. (a)-(g) PL spectra measured for Si/HB/Au nanocavities composed of Si nanoparticles with different diameters at different laser powers. The PL spectra of the HB/Au measured under the same conditions are provided for comparison.

Supplementary Note 8

In Figure S8a,d, we show the forward scattering spectra of two typical Si/HB/Au nanocavities (denoted as A and B) exhibiting enhanced PL intensities (see Figure S8b,e). The PL decays observed for the two Si/HB/Au nanocavities and the reference HB/Au are presented in Figure S8c,f. In each case, the PL decays of both the Si/HB/Au nanocavity and the reference HB/Au can be fitted by biexponential functions. The PL lifetime can be extracted from the time constant of the fast decay component, which is the dominant one.[8] In both cases, it was found that the PL lifetime is reduced in the presence of the Si nanoparticle. Combined with the enhanced PL intensity, the reduction in the PL lifetime in the embedded HB can be attributed to the Purcell effect induced by the Si/Au nanocavity. For nanocavity A, the optical resonance (i.e., MMD) is close to the exciton/trion resonance. In this case, the reduction in the PL lifetime appears to be significant. In comparison, the optical resonance supported by nanocavity B locates at the short-wavelength side of the exciton resonance, implying a relatively weaker Purcell effect. As a result, the shortening of the PL lifetime is not obvious.

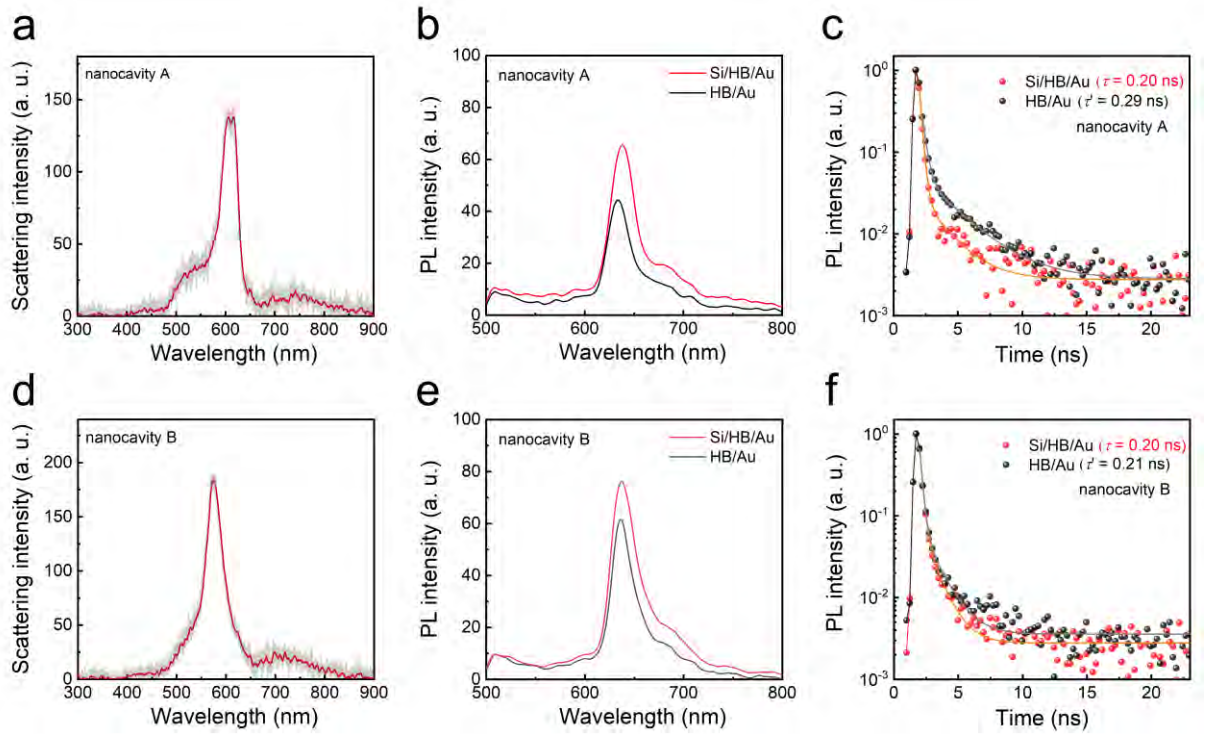

Figure S8. (a)(d) Forward scattering spectra measured for two Si/HB/Au nanocavities (denoted as nanocavity A and B) composed of Si nanoparticles with different diameters. (b)(e) PL spectra of the two Si/HB/Au nanocavities and the reference HB/Au. (c)(f) PL decays measured for the two Si/HB/Au nanocavities and the reference HB/Au (solid symbols) and the fittings with biexponential functions (solid curves).

Supplementary Note 9

In Figure S9, we show the PL spectra of a Si/HB/Au nanocavity (No. 6) and a HB/Au obtained under the excitation of 520-nm femtosecond laser pulses. One can see the reduced PL intensity of the Si/HB/Au at different laser powers, similar to that observed under the excitation of 488-nm CW laser light.

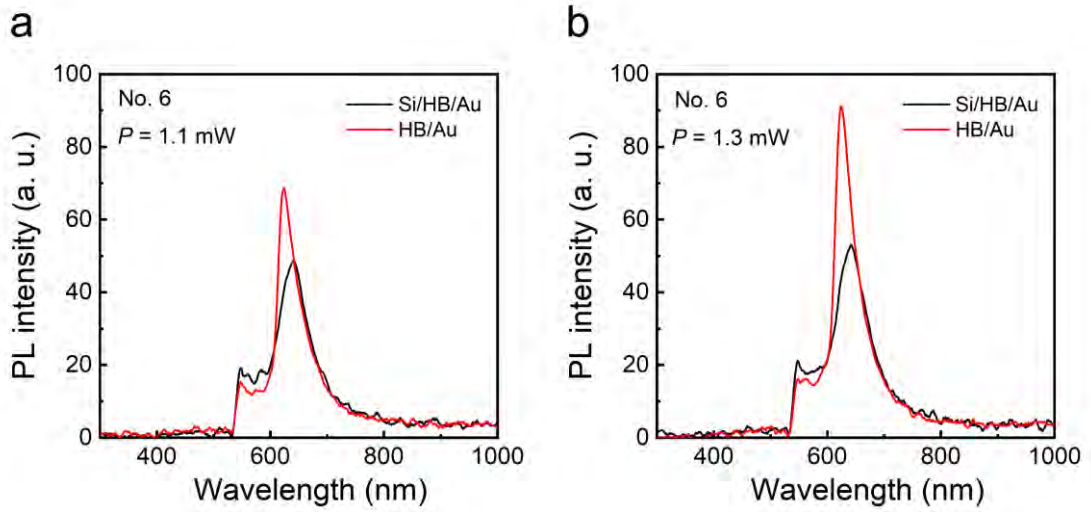

Figure S9. (a)(b) PL spectra of a Si/HB/Au nanocavity (No. 6) and a HB/Au obtained under the excitation of 520-nm femtosecond laser pulses.

Supplementary Note 10

In Figure S10, the dependences of the resonant wavelengths of excitons and trions in the Si/HB/Au nanocavity (No. 7) and HB/Au on the laser power are presented. One can see that the resonant wavelengths of excitons and trions are shifted to longer wavelengths with increasing the laser power. It is noticed that the resonant wavelength of excitons (trions) in Si/HB/Au nanocavity exhibits a ~7 nm redshift as compared with that of the HB/Au at a high laser power of P = 1.26 mW.

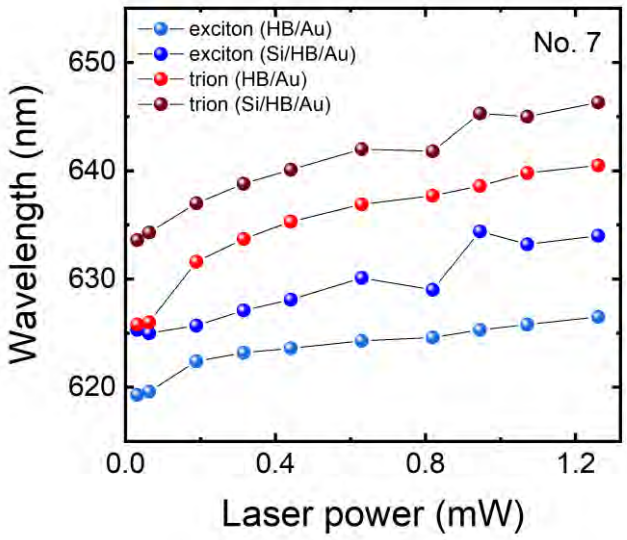

Figure S10. Dependences of the resonant wavelengths of excitons and trions on the laser power extracted from the decompositions of the PL spectra measured for the Si/HB/Au nanocavity (No. 7) and HB/Au.

Supplementary Note 11

In Figure S11, we show the dependence of the relative PL intensity on the laser power observed for a large Si/HB/Au nanocavity (No. 8). It can be seen that the reduction in the PL intensity is small (~20%) and it is not sensitive to the laser power. We suspect that the morphology of the Si nanoparticle is not regular and the induced strain is relatively small. The slight reduction in the PL intensity at high laser powers is caused mainly by the temperature rise in the Si/HB/Au nanocavity.

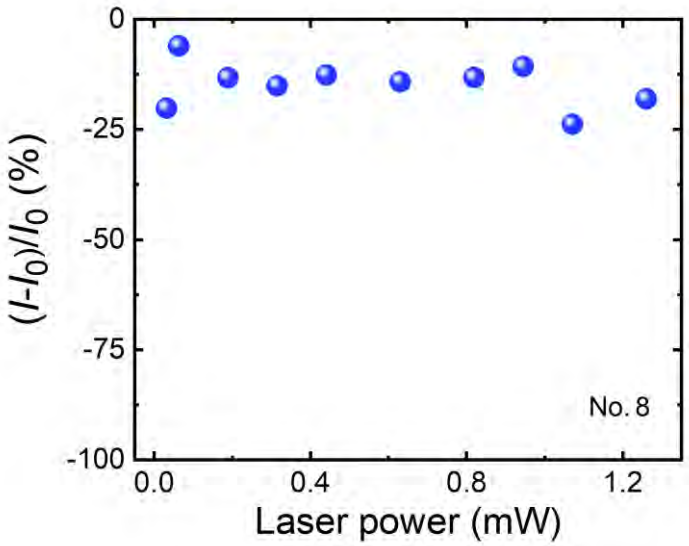

Figure S11. Dependence of the relative PL intensity ($(I-I_0)/I_0$) on the laser power observed for the Si/HB/Au nanocavity (No. 8).

Supplementary Note 12

In Figure S12, we present the dependence of the relative intensity on the laser power observed for excitons and trions in different Si/HB/Au nanocavities. In Figure 4a, it can be seen that the wavelength of excitons in the Si/HB/Au nanocavity (No. 3) moves away from the plasmon resonance, resulting in the decrease of the Purcell factor. Therefore, one can see the decrease of the relative intensity of excitons with increasing laser power (see Figure S12a). In comparison, the change in the relative intensity of trions is not obvious. For the Si/HB/Au nanocavity (No. 4) shown in Figure S12b, the wavelength of excitons approaches the plasmon resonance while that of trions moves away from the plasmon resonance. As a result, one can see the increase in the relative intensity of excitons and the decrease of the relative intensity of trions with increasing the laser power. In the Si/HB/Au (No. 5) shown in Figure S12c, it is observed that the relative intensities of both excitons and trions increase with increasing the laser power. The approaching of the exciton resonance to the plasmon resonance is responsible for the increase in the intensity of excitons. In contrast, the increase in the intensity of trions is caused by the increase in the number of trions because the wavelength of trions moves slightly away from the plasmon resonance. Therefore, we demonstrate that the emission intensities of excitons and trions can be dynamically manipulated.

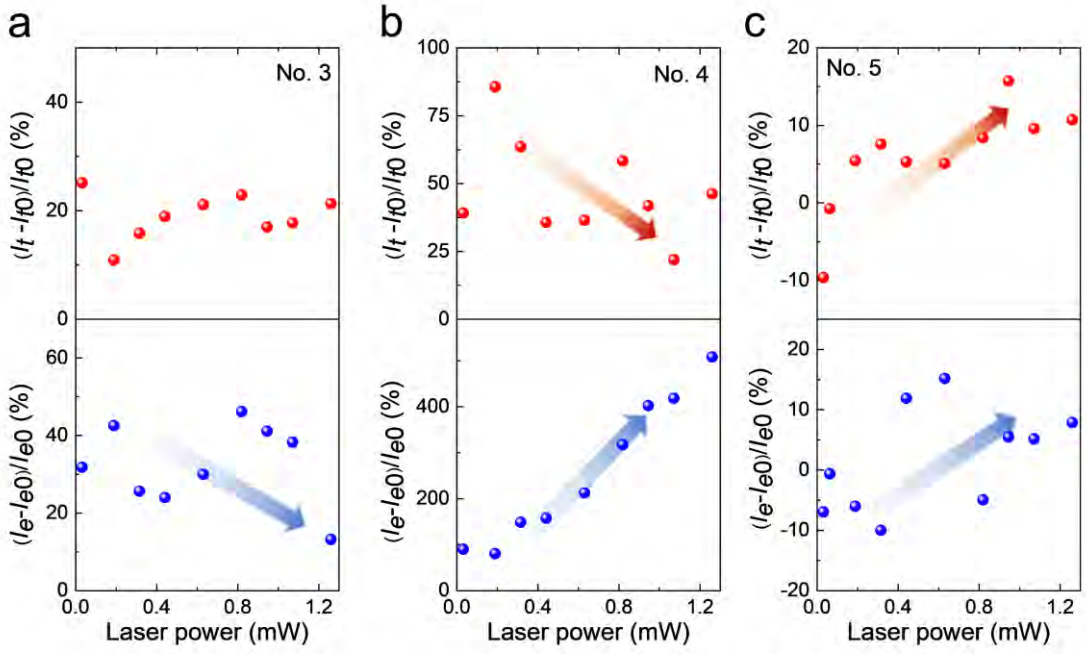

Figure S12. Evolutions of the relative intensities of excitons and trions with increasing laser power observed for three Si/HB/Au nanocavities composed of Si nanoparticles (No. 3, No. 4, and No. 5) with different diameters.

References

[1] G. Lomboy, S. Sundararajan, K. Wang, S. Subramaniam, *Cem. Concr. Res.* **2011**, *41*, 1157.

[2] A. Kawai, T. Yamaji, H. Horiguchi, *J. Photopolym. Sci. Technol.* **2008**, *21*, 85.

[3] Y. Gong, J. Lin, X. Wang, G. Shi, S. Lei, Z. Lin, X. Zou, G. Ye, R. Vajtai, B. I. Yakobson, H. Terrones, M. Terrones, B. K. Tay, J. Lou, S. T. Pantelides, Z. Liu, W. Zhou, P. M. Ajayan, *Nat. Mater.* **2014**, *13*, 1135.

[4] X. Hong, J. Kim, S. F. Shi, Y. Zhang, C. Jin, Y. Sun, S. Tongay, J. Wu, Y. Zhang, F. Wang, *Nat. Nanotechnol.* **2014**, *9*, 682.

[5] H. Li, Y. Xu, J. Xiang, X. F. Li, C. Y. Zhang, S. L. Tie, S. Lan, *Nanoscale* **2016**, *8*, 18963.

[6] S. Liu, F. Deng, W. Zhuang, X. He, H. Huang, J. D. Chen, H. Pang, S. Lan, *ACS Nano* **2022**, *16*, 14390.

[7] H. Huang, F. Deng, J. Xiang, S. Li, S. Lan, *Appl. Surf. Sci.* **2021**, *542*, 148660.

[8] M. Tebyetekerwa, T. N. Truong, W. Yan, C. Tang, A. A. Wibowo, J. Bullock, A. J. Du, C. Yan, D. Macdonald, H. T. Nguyen, *Adv. Mater. Interfaces* **2022**, *9*, 2201649.